

Energy-Efficient Power Control for Multiple-Task Split Inference in UAVs: A Tiny Learning-Based Approach

Chenxi Zhao, Min Sheng, *Senior Member, IEEE*, Junyu Liu, *Member, IEEE*, Tianshu Chu, and Jiandong Li, *Fellow, IEEE*

Abstract—The limited energy and computing resources of unmanned aerial vehicles (UAVs) hinder the application of aerial artificial intelligence. The utilization of split inference in UAVs garners significant attention due to its effectiveness in mitigating computing and energy requirements. However, achieving energy-efficient split inference in UAVs remains complex considering of various crucial parameters such as energy level and delay constraints, especially involving multiple tasks. In this paper, we present a two-timescale approach for energy minimization in split inference, where discrete and continuous variables are segregated into two timescales to reduce the size of action space and computational complexity. This segregation enables the utilization of tiny reinforcement learning (TRL) for selecting discrete transmission modes for sequential tasks. Moreover, optimization programming (OP) is embedded between TRL's output and reward function to optimize the continuous transmit power. Specifically, we replace the optimization of transmit power with that of transmission time to decrease the computational complexity of OP since we reveal that energy consumption monotonically decreases with increasing transmission time. The replacement significantly reduces the feasible region and enables a fast solution according to the closed-form expression for optimal transmit power. Simulation results show that the proposed algorithm can achieve a higher probability of successful task completion with lower energy consumption.

Index Terms—Power control, tiny learning, energy-efficient, multiple-task split inference.

I. INTRODUCTION

In recent years, there has been a remarkable surge in the proliferation of unmanned aerial vehicles (UAVs), accompanied by the deployment of diverse delay-sensitive applications on UAVs, e.g., surveillance and exploration [1], [2], where UAVs can send the data through the satellite network or cellular network [3], [4]. For expediting access to and processing of the data from UAVs, the widespread implementation of artificial intelligence (AI) technologies in UAVs is imperative. The concept of aerial AI refers to the implementation of deep neural networks (DNN) on UAVs, thereby facilitating localized provision of AI services that empower emerging applications at Internet of UAVs. However, the deployment of aerial AI on UAVs is hindered by constraints in energy and computing capabilities.

The split inference is a state-of-the-art AI architecture, wherein the DNN is divided into device and server sub-models [5]–[7]. Utilizing the device sub-model, a UAV extracts features from raw data samples and transmits them to a server. Subsequently, the server employs these features to compute

an inference result. The utilization of split inference can significantly alleviate the computation load on UAVs, thereby reducing energy consumption. Nevertheless, there are some challenges associated with the application of split inference. Specifically, ensuring the delay constraint becomes challenging under direct data transmission, while transmitting data features after processing significantly increases energy consumption. The delay constraint and energy consumption of split inference poses a complex trade-off. Worststill, the coupling among multiple sequential tasks and the random time-varying wireless channel further complicate the aforementioned issue. Therefore, this work focuses on 1) how to choose whether to apply split inference based on the current energy level of UAV and task delay constraint, and 2) optimizing the resource allocation policy for multiple tasks considering the random time-varying wireless channel.

A. Related Work and Motivation

Extensive research has been conducted on the edge AI problem, and comprehensive surveys on this topic can be found in [8]–[12]. In [8], authors propose an on-demand DNN collaborative inference framework, wherein edge devices collaborate to achieve low latency edge AI. Similarly, a multi-device edge computing framework is proposed in [9], where the task execution of multi-device edge computing is defined as a multi class classification problem. Moreover, a hardware-based prototype and a software framework for optimizing a pre-trained YOLOv2 model is introduced in [10] to achieve lower inference latency for a single input by collating partial outputs generated by partitioned CNN parameters at the gateway device. In [11], the memory and communication requirements of edge devices are optimized considering the limited computing resources of most edge computing devices. While these efforts explore the potential of edge AI to significantly enhance performance in various aspects for edge devices, they fail to acknowledge the crucial constraints posed by limited energy and computing capabilities of such devices, which are critical considerations in practical deployments of edge AI, especially for UAVs.

Considering the fact that UAVs typically lack an external power supply, energy harvesting is commonly employed in UAVs to facilitate long-term sustained operation, e.g., radio-frequency energy harvesting and solar energy harvesting [13]–[17]. In [13], a UAV-aided multiaccess edge computing system

with energy harvesting is studied, where the full-duplex protocol is considered to realize simultaneously receiving confidential data from the UAV and broadcasting the control instructions. A novel model that uses a cluster of UAVs with energy harvesting capability as a computational core is constructed in [14]. It is capable of providing long-term computational services for various scenarios. In [15], a UAV-enabled mobile-edge computing (MEC) wireless-powered system is studied. The computation rate maximization problems in a UAV-enabled MEC wireless powered system are investigated under both partial and binary computation offloading modes, subject to the energy-harvesting causal constraint and the UAV's speed constraint. In [16], authors considered an online dynamic offloading and resource scheduling algorithm to address the stochastic optimization problem of minimizing energy and computing resource consumption of energy harvesting devices while meeting the quality of service requirements of IoT devices. However, while energy harvesting can extend the device's uptime, it does not mitigate the energy consumption of edge AI. Insufficient harvested energy still impacts edge AI operations, and the instability in its collection significantly affects performance.

The split inference is an advanced edge AI architecture designed to optimize energy consumption in edge devices [5], [18]–[20]. Specifically, the overall model is partitioned into two components, with one part being processed by the edge device and the other by the server. It is important to note that the split inference approach differs from the part offload model in edge computing, as the latter partitions the data into two segments while still executing the entire AI model on the edge device. In contrast to the part offload model, split inference offers a significant reduction in computation and communication overhead as well as ensuring data privacy. In [21], authors study the joint optimization of the model placement and online model splitting decisions to minimize the energy-and-time cost of device-edge co-inference in presence of wireless channel fading. A multi-agent collaborative inference scenario, including a single edge server and multiple user equipment (UEs), is studied in [22] to achieve fast and energy-efficient inference for all UEs. In [23], authors consider the scenario including multiple application tasks with different options of deep learning models and different hyperparameter settings. Although significant achievements have been made by combining split inference with edge task offloading, the potential impact of coupling among multiple sequential tasks is often overlooked. Moreover, the adverse effects of random time-varying wireless channels can further exacerbate the coupling above.

As previously discussed, in order to fully harness the advantages of split inference and reduce the energy consumption, it is imperative to address two key considerations before applying split inference in UAVs. On the one hand, the energy level of UAVs and task delay requirements must be taken into account when employing split inference. On the other hand, the selection of transmission mode and transmit power should be jointly optimized considering the randomness of task arrival and time-varying wireless channel parameters. These two challenges serve as the driving force behind this research.

B. Contribution

The energy-efficient power control for multi-task split inference in UAVs is studied in this paper, taking into consideration multiple sequential tasks. Upon the arrival of a task, it is initially determined whether to employ split inference based on energy level of UAVs and task delay constraints. Subsequently, the transmit power in each time slot is optimized to minimize total power consumption while ensuring the delay constraints of all tasks. Furthermore, we develop an optimal algorithm to solve it. The main contributions of this paper can be summarized as follows:

- An optimization programming (OP)-embedded tiny reinforcement learning (TRL) framework is proposed. To be specific, we first present the energy minimization as a two-timescale problem, where discrete and continuous variables are segregated into two timescales. TRL-based approach is utilized to determine whether split inference should be employed for processing tasks based on the energy level of UAVs, length of the transmission queue and task arrival rate. Furthermore, an OP is embedded between the output and reward function of TRL to optimize the transmit power in each time slot. Compared to conventional deep reinforcement learning (DRL)-based algorithms, the proposed framework can significantly decrease the size of action space and training time.
- An optimal algorithm is developed to optimize the transmit power in each time slot. In particular, the sample average approximation method is applied to address the chance constraint caused by the random wireless channel parameters. Then, the alternating direction method of multipliers (ADMM) method is explored to transform the initial problem into multiple subproblem to decrease the complexity. For each subproblem, the minimal transmit power is achieved by optimizing the transmission time of each task, which is motivated by our findings that increasing transmission time leads to a monotonic decrease in energy consumption. The substitution significantly reduce the feasible region and enables fast solution according to the closed-form expression for optimal transmit power. Simulation results show that the proposed OPETRL can achieve a higher probability of successful data transmission with lower overall energy consumption.

The rest of this paper is organized as follows. Section II introduces the system model. The problem formulation and transformation are given in Section III. The OP-embedded TRL architecture and the optimal algorithm for transmit power are given in Section IV. Section VI shows the simulation results and Section VI concludes this paper.

II. SYSTEM MODEL

A. Network Model

Consider the edge inference system shown in Fig. 1, which consists of a UAV and a server. The UAV is equipped with some sensors and collects the raw data, such as images for surveillance. Then, the local data at UAV is compressed into features and sent to the server to do a remote inference on a trained model. The considered the UAV is powered by the

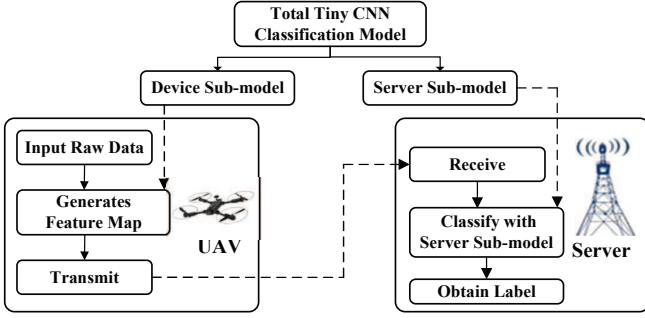


Figure 1. The split inference system in UAVs.

harvested solar energy. The amount of harvested solar energy is affected by clouds [24], where the harvested solar energy is reduced if there is a cloud between the sun and the solar panel. The attenuation of the solar light passing through a cloud can be modeled as [24]

$$\phi(d_{\text{cloud}}) = e^{-\beta d_{\text{cloud}}}, \quad (1)$$

where $\beta \geq 0$ denotes the absorption coefficient that models the optical characteristics of cloud and d_{cloud} denotes the cloud thickness. Therefore, the output power of the solar panel used by the UAV can be modeled by the following function

$$P_s = \eta S G e^{-\beta d_{\text{cloud}}}, \quad (2)$$

where η and S are constants that denote the energy harvesting efficiency and the equivalent area of the solar panels, respectively. Moreover, G denotes the average solar radiation intensity on earth. Note that (2) is a simplified model that ignores the change of G over time during the day. The reasonableness of this assumption lies in the fact that the duration of data transmission is significantly shorter than the change period of G . Therefore, in this paper, we consider the output power of the solar panel used by the UAV is a constant.

B. Transmission Model

A tiny CNN classification model is applied in this paper, which comprises multiple convolutional (CONV) layers followed by multiple fully-connected layers. We consider two patterns to complete classification tasks. For the first pattern, the UAV transmit directly the raw data to the server, called direct transmission (DT) pattern. The size of raw data is set as S bits. In this case, the total tiny CNN classification model is deployed in the server. For the second pattern, the UAV generates the feature map of raw data and sends the feature map to the server, called computation-transmission (CT) pattern. In this case, the classification model should be divided into two parts to implement split inference, i.e., device sub-model and server sub-model. Following the widely used designs [5], [18], the splitting point is set after the CONV layers, where the output of the last CONV layer is a feature map with height L_h and width L_w . Each element in the feature map is quantized with a sufficiently high resolution of Q bits such that quantization errors are negligible. Note that the completion time for classification tasks generally has a requirement, although it may be less stringent in certain

applications, such as surveillance. We denote C as the task completion time threshold, which means that the duration from acquiring the raw data to obtaining the classification result should be within C . The processing time on the server is disregarded in this paper, as it is reasonable to assume that the server possesses ample computing power and is not constrained by any power limitations. Consequently, compared to the processing time on the UAV and transmission delay, the processing time on the server can be considered negligible.

The UAV is allocated a narrow-band channel, whose bandwidth is denoted by W . The time of the considered system is divided into multiple time slots, whose set is denoted by $\mathcal{T} = \{1, \dots, T\}$. In particular, the duration of each time slots is denoted by τ , which is smaller than the coherence time of the communication channel. Thus, the power gain of wireless channel is constant within each time slot. Denote g_t as the small-scale fading channel coefficient between the UAV and server at time slot t . In particular, g_t is an independent and identically distributed (i.i.d.) random variable over time slots, where the distribution function of $g(t)$ is set as \mathcal{P}_g . Moreover, we consider the zero-mean Gaussian noise with variance σ^2 . Therefore, the achievable rate of the channel between the UAV and server at time slot t can be expressed as

$$R_t = W \log_2 \left(1 + \frac{p_t g_t}{\sigma^2 d^2} \right), \quad (3)$$

where p_t and d are the transmit power at time slot t and the distance from the UAV to server, respectively.

C. Energy Model

To capture the key features of the energy consumption during computation and communication in the edge inference system, the energy consumption model is first studied in this section. Specifically, we focus on energy consumption during data transmission and processing in the UAV, which are elaborated as follows.

- **Computing Energy:** For CT pattern, the UAV need to generate the feature map of raw data. Denote c as the number of floating-point operations required to generate the feature map, which is depended on the architecture of CNN deployed in the UAV. Moreover, denote n_t as the number of floating-point operations required by all CONV layers. The computing power of UAV at time slot t is modeled as $p_t^C = k f^3$ as in [25], where f and k are the UAV's computational speed and a coefficient depending on chip architecture, respectively. Denote f_{\max} as the maximum computational speed of UAV. The number of floating-point operations that the UAV can handle in a cycle is modeled as $n_d = N_c n_v / n_s$, where N_c and n_s are the number of CPU cores and the bit size of operating system, respectively. In addition, n_v is the bits of vector operation in each cycle. Therefore, the execution time of generating the feature map is $t_f^C = \frac{n_t n_s}{f N_c n_v}$. The energy consumption of generating the feature map is given by

$$E^C = \frac{k f^2 n_t n_s}{N_c n_v}. \quad (4)$$

- **Transmission Energy:** Denote t_i^S and t_i^T as the start time of transmission and the time consumption of transmission

for the i -th raw data or its feature map, respectively. Thus, the transmission energy consumption is $E^T(i) = \sum_{t=t_i^S}^{t_i^T} p_t^T$.

Besides the energy consumption, we also model the battery energy level of UAV. Denote E_t^B as the battery energy level of UAV at the start of time slot t . Thus, E_0^B is the initial energy level of UAV. During each time slot t , the UAV receives a finite amount of energy, i.e., τP_s , from the environment. Therefore, the energy in the battery at the start of time slot $t+1$ epoch is given by

$$E_{t+1}^B = E_t^B + \tau P_s - E_t^T - E_t^C, \forall t \quad (5)$$

where E_t^T and E_t^C are the transmission energy consumption and the computing energy consumption at time slot t , respectively.

D. Traffic Model

We assume that the sensor will generate the raw data at each time slot with probability q . Denote $a_t = 1$ as the raw data is generated at time slot t , while the time slot that the i -th raw data arrives is denoted by t_i^A . As mentioned in Section II-B, the UAV will choose one pattern to process the raw data after it is generated. For DT pattern, the UAV directly puts the raw data into the transmission queue and process the next raw data. However, for CT pattern, the UAV first gets the feature map and put it into the transmission queue and then, processes the next raw data. Let the computational variable $b_t \in \{0, 1\}$ indicate that whether the UAV process the raw data generated at time slot t with DT pattern. If yes, $b_t = 1$; else $b_t = 0$. Furthermore, the UAV will choose a computational speed to process the raw data if $b_t = 1$. To guarantee the task completion time threshold C , the transmit power p_t should satisfy the following constraint

$$\tau \sum_{t=0}^{t_i^A+C} R_t \geq \sum_{t=0}^{t_i^A} a_t [b_t L_h L_w Q + (1 - b_t) S], \forall i. \quad (6)$$

Meanwhile, the transmit power p_t should satisfy the following causal constraint

$$\tau \sum_{t=0}^{t_i^S+t_i^T} R_t \leq \sum_{t=0}^{t_i^A} a_t [b_t L_h L_w Q + (1 - b_t) S], \forall i. \quad (7)$$

III. PROBLEM FORMULATION

In this section, we formulate the optimization problem to minimize the energy consumption of UAV and then, transform it into a multistep decision problem.

A. Problem formulation

We first formulate a problem to minimize the energy consumption of UAV as follows

$$\begin{aligned} \text{(P0)} \quad & \min_{\mathbf{p}, \mathbf{b}, \mathbf{f}} \sum_t (E_t^T + E_t^C) \\ \text{s.t.} \quad & 0 \leq E_t^B \leq E_{\max}^B, \forall t, \quad (8) \\ & 0 \leq f_i \leq f_{\max}, \forall i, \quad (9) \\ & b_t \in \{0, 1\}, \forall t, \quad (10) \\ & b_t \leq a_t, \forall t, \quad (11) \\ & 0 \leq p_t \leq p_{\max}, \forall t, \quad (12) \\ & (7), (6). \end{aligned}$$

where $\mathbf{p} = \{p_1, \dots, p_t\}$ and $\mathbf{b} = \{b_1, \dots, b_t\}$ are the sets of transmit power and computational variables. In addition, $\mathbf{f} = \{f_1, \dots, f_i\}$ is the set of UAV computational speed for different tasks. In problem (P0), constraint (8) means that the energy in the battery should be positive and smaller than the maximum battery capacity, denoted by E_{\max}^B . Constraint (6) indicates that each task i should be completed within the time threshold C . Moreover, constraint (7) is a causal constraint where the transmission process of the i -th raw data cannot be earlier than its generation time. Constraints (6) and (7) make problem (P0) quite different from other single-task optimization problems, where the summation upper limits in the two constraints are dependent on the previous resource allocation, thereby making the two constraints a form of uncertainty. In particular, denote t_i^{QC} and t_i^{QT} as the queuing delay of the i -th raw data in the transmission queue and computation queue, respectively. Thus, the queuing delay of the transmission queue can be written as

$$t_i^{\text{QC}} = \max \left\{ 0, t_{i-1}^A + t_{i-1}^{\text{QC}} + a_t (1 - b_t) t_{f_{i-1}}^C - t_i^A \right\}, \quad (13)$$

where $t_0^{\text{QC}} = 0$. Moreover, the queuing delay of the transmission queue is

$$t_i^{\text{QT}} = \max \left\{ 0, t_i^S - \left(t_i^A + t_i^{\text{QC}} + t_{f_i}^C \right) \right\}, \quad (14)$$

where $t_i^S = t_{i-1}^A + t_{i-1}^{\text{QC}} + t_{i-1}^{\text{QT}} + t_{i-1}^T$.

B. Problem transformation

As mentioned above, problem (P0) differs from one-task optimization problems [25], where the preceding tasks have impact on the pattern choice of subsequent tasks and resource allocation strategies in the subsequent time slots. Meanwhile, problem (P0) is also different from the multi-task optimization problems, which do not consider the task completion time threshold and queuing delay. To solve problem (P0), we

transform it into a series of multistep decision problems, where the problem in the t' -th time slot is shown as

$$(P1) \min_{\mathbf{p}_{t'}, b_{t'}, f} \sum_{t \in \mathcal{I}_{t'}} (E_t^T + E_t^C) \quad (15)$$

$$s.t. \quad b_{t'} \in \{0, 1\}, \quad (16)$$

$$b_{t'} \leq a_{t'}, \quad (16)$$

$$0 \leq E_t^B \leq E_{\max}^B, \forall t \in \mathcal{I}_{t'}, \quad (17)$$

$$0 \leq p_t \leq p_{\max}, \forall t \in \mathcal{I}_{t'}, \quad (18)$$

$$\tau \left(\sum_{t=t_i^S}^{t'-1} \tilde{R}_t + \sum_{t=t'}^{t_i^S+t_i^T} R_t \right) \leq \sum_{t=t'}^{t_i^A} b_t L_h L_w Q + (1 - b_t) S, \forall i \in \mathcal{I}_{t'}. \quad (19)$$

$$\tau \left(\sum_{t=t_i^S}^{t'-1} \tilde{R}_t + \sum_{t=t'}^{t_i^A+C} R_t \right) \geq \sum_{t=t'}^{t_i^A} b_t L_h L_w Q + (1 - b_t) S, \forall i \in \mathcal{I}_{t'} \quad (20)$$

In problem (P1), it is defined that $\mathcal{I}_{t'} = \{i | t_i^A \leq t'\}$, $\mathcal{I}_{t'} = \{t', \dots, t_i^A + C | i = \arg \max_i \{t_i^A \leq t'\}\}$ and $\mathbf{p}_{t'} = \{p_t^T | t \in \mathcal{I}_{t'}\}$. Moreover, we set $f = 0$ if $b_{t'} = 0$. Note that \tilde{R}_t are known in the t' -th time slot, which are dependent on the process strategy and power allocation before the t' -th time slot.

While the initial problem (P0) can be transformed into a series of multistep decision problems, problem (P1) is still intractable. In the next section, an algorithm is designed for the multistep decision problems.

IV. TINY LEARNING ARCHITECTURE-BASED OPTIMAL ALGORITHM

In practice, problem (P1) should be solved within a short time, while the UAV generally does not have enough computation capacity to finish it within the predefined time. DRL is a promising method to achieve fast strategy generation. However, problem (P1) is a mixed integer programming (MIP). While MIP can be solved by DRL, a complex neural network (NN) with massive parameters is necessary. It is impractical to deploy a complex NN in the UAV due to the limited energy. Hence, in this section, we propose a tiny reinforcement learning (TRL) architecture, which can significantly reduce the number of parameters of NN via embedding the optimization programming into TRL. Furthermore, the complexity of optimization programming is also greatly decreased by analyzing the non-linear objective function.

A. TRL-based architecture

As discussed above, problem (P1) is a MIP problem. It is unsuitable for UAVs to apply DRL to solve the MIP problem due to the massive parameters of NN. Recalling and carefully analyzing problem (P1), we find that it is not

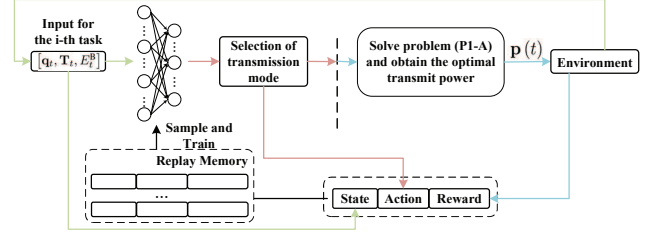


Figure 2. The TRL-based architecture.

necessary to include the continuous variables into the action space of the NN in reinforcement learning. Specifically, the discrete variables in problem (P1) determine the strategies for transmission modes in the sequential time slots, while the continuous variables determine the allocation of transmission power in each timeslot. As is widely acknowledged, reinforcement learning excels at addressing continuous decision problems due to its inherent MDP nature. Therefore, if the optimal solution for transmission power allocation in each time slot can be achieved under the given strategies for completing task patterns, it would enable the separation of continuous and discrete variables in problem (P1). In this case, employing only reinforcement learning to determine the discrete variables for transmission mode selections within the sequential time slots would significantly simplify the NN structure utilized in reinforcement learning. Additionally, optimizing the continuous variables of transmission power allocation can circumvent MIP, thereby substantially reducing computational time. The proposed TRL architecture, called OP embedded TRL (OPETRL), is given in Fig. 2.

The problem (P1-A) in Fig. 2 is given as follows

$$(P1-A) \min_{\mathbf{p}_{t'}} \sum_{t \in \mathcal{I}_{t'}} (E_t^T + E_t^C) \quad (17) - (20).$$

In problem (P1-A), the computational variable b_t is fixed, which distinguishes it from problem (P1). The key ideas of OPETRL include two aspects. On the one hand, the solution processes of continuous and discrete variables are segregated, with OP and TRL employed for their respective resolutions. This segregation is critical as the presence of mixed-integer variables can significantly reduce the convergence rate of DRL and increase computational time required by OP. On the other hand, the reward is not obtained by directly implementing action in the environment. The action of TRL is considered as the input of OP, whose output determines the reward of TRL in conjunction with the action. In the following, we will provide a detailed description of both TRL and OP.

B. TRL for transmission mode selection

As previously mentioned, TRL is employed to determine strategy for selecting transmission modes. In this paper, we utilize DDQN, providing a detailed exposition of the state space, action space, reward function, and network architecture in subsequent sections.

1) *State space*: The state in time slot t is denoted by $\mathbf{s}_t = [\mathbf{q}_t, \mathbf{T}_t, E_t^B]$, where \mathbf{q}_t represents the vector of the data size of each task awaiting transmission and \mathbf{T}_t denotes the vector of remaining time allowed to complete each task. In each time slot, the NN in DRL selects a transmission mode based on the transmission queue, time threshold and the energy level upon task arrives.

2) *Action space*: Observing the state, the NN in DRL outputs the decision of transmission mode at each time slot. The action for the i -th task is defined as $a(t)$, where the size of action space equals 2. The action will be regarded as the input of problem (P1-A), whose output further determines the reward of agent.

3) *Reward function*: The reward for the i -th task, denoted by $r(i)$, is contingent upon the violation of constraints during a task. Specifically, the action violating the completion time constraint will be penalized with a negative reward, while adherence to it will result in a positive reward. Note that the action choosing transmission modes varies in a long-timescale manner, while the transmit power varies in a short-timescale manner. Hence, the reward will not be generated at each time slot. The reward for the i -th task is set as the energy consumption in duration $[t_i^A, t_i^S + t_i^T]$.

4) *Network Architecture*: In this paper, DDQN is used to determine the transmission mode for each task [26]. There are one fully-connected hidden layers with 32 neurons in the Q network. The ReLU is used as an activation function in hidden layer. The parameter of the Q network is initialized by a Xavier initialization scheme [27]. Besides, the target Q network is created by copying the corresponding parameters of the Q network in the initialization phase.

The replay memory is updated with a new training sample $(\mathbf{s}(i), a(i), r(i), \mathbf{s}(i+1))$ when the i -th task is completed within the time threshold or reaches the time threshold. While updating the network parameters, a random minibatch of training samples are sampled uniformly from replay memory. The replay memory size is 1000 and the minibatch size is 64. The Q network is trained by using the gradient descent method to minimize the loss function, which is defined as the mean square error of the difference between the Q value given by Q network and the target value given by the target Q network. Moreover, the parameters of the Q network will be copied into the target Q network each 20 time steps.

C. Optimal algorithm for transmit power

After determining the transmission mode, problem (P1-A) should be addressed in order to obtain a resource allocation strategy that satisfies the time threshold of each task. However, the inherent randomness of wireless channels, which results in random achievable transmit rate, poses a challenge in meeting time threshold constraint (19). To solve it, we reformulate time threshold constraint (19) as a chance constraint, which is given

by

$$\Pr \left\{ \tau \left(\sum_{t=t_i^S}^{t'-1} \tilde{R}_t + \sum_{t=t'}^{t_i^A+C} R_t \right) \geq \sum_{t=t'}^{t_i^A} a_t [b_t L_h L_w Q + (1 - b_t) S] \right\} \geq 1 - \epsilon, \forall i \in \mathcal{I}_{t'} \quad (21)$$

In (21), $0 < \epsilon \ll 1$ is the maximum probability that the time threshold constraint cannot be satisfied. Moreover, the objective function in problem (P1-A) is also reformulated as

$$\mathbb{E}_{\mathbf{g} \sim \mathcal{P}_g} \left[\sum_{t \in \mathcal{I}_{t'}} E_t^T \right]. \quad (22)$$

Hence, problem (P1-A) can be rewritten as

$$\begin{aligned} \text{(P1-B)} \quad & \min_{\mathbf{p}_{t'}} \mathbb{E}_{\mathbf{g} \sim \mathcal{P}_g} \left[\sum_{t \in \mathcal{I}_{t'}} E_t^T \right] \\ & \text{s.t. (17) - (19), (21)}. \end{aligned}$$

1) *Problem transformation*: Problems (P1-B) is difficult to solve exactly since it is difficult to obtain the closed-form expressions of (21). To solve it, we approximate the computationally intractable chance constraints (21) via the sample average approximation (SAA) technique [28], [29]. The SAA technique offers two advantages in approximating chance constraints. On the one hand, it is applicable to general channel distribution models, which is crucial as the practical distribution of channel coefficients often defies typical modeling approaches. On the other hand, by replacing the chance constraint with a finite set of simpler constraints under the SAA technique, we can ensure that the performance gap between solutions to the sample approximation problem and those to the original problem remains minimal. Denote \mathbf{g}^k as the k -th independent sample of \mathbf{g} generated according to \mathcal{P}_g , where $k \in \mathcal{K}$ with $\mathcal{K} \triangleq \{1, \dots, K\}$. According to the law of large numbers, if the sample size K is sufficiently enough, we can approximately substitute the objective functions in problems (P1-B) with

$$\mathbb{E}_{\mathbf{g} \sim \mathcal{P}_g} \left[\sum_{t \in \mathcal{I}_{t'}} (E_t^T + E_t^C) \right] \approx \frac{1}{K} \sum_{k \in \mathcal{K}} \sum_{t \in \mathcal{I}_{t'}} (E_t^{T,k} + E_t^{C,k}). \quad (23)$$

Moreover, the chance constraint (21) can be replaced with

$$\begin{aligned} & \tau \left(\sum_{t=t_i^S}^{t'-1} \tilde{R}_t + \sum_{t=t'}^{t_i^A+C} R_t^k \right) \\ & \geq \sum_{t=t'}^{t_i^A} a_t [b_t L_h L_w Q + (1 - b_t) S], \forall i \in \mathcal{I}_{t'}, k \in \mathcal{K}. \end{aligned} \quad (24)$$

It has been proved that if the number of samples K is no less than K^* with

$$K^* = \left\lceil \frac{1}{\epsilon} \left(N - 1 + \log \frac{1}{\theta} \sqrt{2(N-1) \log \frac{1}{\theta} + \log^2 \frac{1}{\theta}} \right) \right\rceil \quad (25)$$

for any $\theta \in (0, 1)$, then any solution satisfying constraint (24) may satisfy chance constraint (21) with a probability at least $1 - \theta$ [28], [29].

The number of variables and constraints in the transformed problem is significantly larger (approximately K times that of problem (P0)), particularly when dealing with a large number of samples K . Moreover, it should be noted that the transformed problem represents a non-convex optimization problem with constraint (19). However, due to limited computational capacity and energy resources, the UAV is unable to achieve a solution within a time slot. To handle it, we reframe it as a global consensus problem [30], which is prevalent in the domains of distributed computing and multi-agent systems, necessitating all agents to converge on a shared value crucial for computation. In the transformed problem, we focus on optimizing the transmit power and computational speed under random channel coefficients, where the optimization of the computational speed executes once after task arrival. Therefore, we can consider each sample as an individual agent, with the transmit power at the current time slot being treated as a shared variable among all agents. Inspired by the approaches in [31], a parallel architecture is proposed for problem (P1-B). To be specific, we replace problem (P1-B) as K subproblems, where the k -th subproblem is

$$\begin{aligned} \text{(P1-C)} \quad & \min_{\mathbf{p}_{t'}^k} \sum_{t \in \mathcal{I}_{t'}} E_t^{\Gamma, k} \\ & \text{s.t. (17) - (19),} \\ & \tau \left(\sum_{t=t_i^S}^{t'-1} \tilde{R}_t + \sum_{t=t'}^{t_i^A+C} R_t^k \right) \\ & \geq \sum_{t=t'}^{t_i^A} a_t [b_t L_h L_w Q + (1 - b_t) S], \forall i \in \mathcal{I}_{t'}. \quad (26) \end{aligned}$$

Note that the variables in constraints (17)-(19) within problem (P1-C) are the corresponding ones under the sample \mathbf{g}^k . To obtain the transmit power, we can parallelly address the K subproblems and then recover $\mathbf{p}_{t'}$ and f from the solutions via ADMM. In the following, we present the optimal algorithm for each subproblem.

2) *Optimal algorithm for subproblem:* We aim to propose an algorithm that can efficiently achieve the solution for problem (P1-C) with low computational complexity. However, constraint (19) is a non-convex constraint, which results in extra computational complexity. Therefore, we present a problem

formulation for the transmission of the i -th task as follows

$$\begin{aligned} \text{(P2)} \quad & \min_{\mathbf{p}_{t_i^S}^k} \sum_{t=t_i^S}^{t_i^S+t_i^{\Gamma, \max}} p_t^k \\ & \text{s.t. (18),} \\ & \tau \sum_{t=t_i^S}^{t_i^S+t_i^{\Gamma}} R_t^k \geq D_i, \quad (27) \end{aligned}$$

where $D_i = b_{t_i^A} L_h L_w Q + (1 - b_{t_i^A}) S$, $\mathbf{p}_{t_i^S}^k = (p_{t_i^S}^k, \dots, p_{t_i^S+t_i^{\Gamma, \max}}^k)$ and $t_i^{\Gamma, \max}$ is the allowed transmission time of the i -th task. Note that in problem (P2), the time consumption of transmission for the i -th task is given. By the Karush-Kuhn-Tucker (KKT) conditions, the sufficient and necessary conditions for the optimal solution of problem (P2), denoted by $\mathbf{p}_{t_i^S}^k$, can be stated in the following theorem.

Theorem 1. *The optimal solution $\mathbf{p}_{t_i^S}^{k,*}$ of problem (P2) satisfies the following sufficient and necessary conditions*

$$p_t^{k,*} = \min \left\{ \left[\tau W e^{\frac{D_i - \sum_{t=t_i^S}^{t_i^S+t_i^{\Gamma, \max}} \log(\tau W h_t^k)}{t_i^{\Gamma, \max}}} - \frac{1}{h_t^k} \right]^+, p_{\max} \right\} \quad (28)$$

for all $t \in \mathcal{T}_{t_i^S} \triangleq (t_i^S, \dots, t_i^S + t_i^{\Gamma, \max})$, where $h_t^k = \frac{g_t^k}{\sigma^2 d^2}$ and $[x]^+ = \max\{0, x\}$.

Proof. Please refer to Appendix A. \square

Moreover, we proof that the total energy under the optimal solution decreases monotonically with the transmission time in the following theorem.

Theorem 2. *The objective value of problem (P2) associated with the optimal solution decreases monotonically with the transmission time.*

Proof. Please refer to Appendix B. \square

Remark: According to Theorem 1 and 2, the optimal strategy for transmit power can be obtained by optimizing the allowed transmission time of each task. Moreover, the transmission process will last until the completion time threshold of the last task in the current queue is reached.

Hence, we formulate the optimization problem at the t' -th time slot as

$$\begin{aligned} \text{(P3)} \quad & \min_{t_i^{\Gamma, \max}} \sum_{i \in \mathcal{I}_{t'}} E_i(t_i^{\Gamma, \max}) \\ & \text{s.t. } t_i^S + t_i^{\Gamma, \max} \leq t_i^A + C, i \in \mathcal{I}_{t'} \quad (29) \end{aligned}$$

$$t_l^S + t_l^{\Gamma, \max} = t_l^A + C \quad (30)$$

$$t_i^S = t_{i-1}^S + t_{i-1}^{\Gamma, \max}, i \in \mathcal{I}_{t'}, \quad (31)$$

where $E_i(t_i^{\Gamma, \max})$ is the total transmission energy for the i -th task. Moreover, in (30), l is the index of the last task in the set $\mathcal{I}_{t'}$. The optimal solution of problem (P3) should satisfy the condition stated in Theorem 3.

Algorithm 1 Optimal algorithm for transmit power

- 1: **Initialization**
 - 2: • Input task set $\mathcal{I}_{t'}$ and the transmission data of each task $D_i, \forall i \in \mathcal{I}_{t'}$.
 - 3: • Set the allowed transmission time of the first task as $t_1^{T,\max,(0)} = t_1^A + C - \max\{t_1^S, t'\}$.
 - 4: • Set the allowed transmission time of other tasks as $t_i^{T,\max,(0)} = t_i^A + C - t_i^S, \forall i \in \mathcal{I}_{t'} \setminus \{1\}$.
 - 5: • Set $l = 1$.
 - 6:
 - 7: **while** $l < Loop$
 - 8: Calculate the values on both sides of (32), denoted by $f_{n,m}^L$ and $f_{n,m}^R, \forall n, m \in \mathcal{I}_{t'}$, respectively.
 - 9: Set $\{n_{\max}, m_{\max}\} = \arg \max_{n,m} (f_{n,m}^R - f_{n,m}^L)$.
 - 10: **if** $f_{n_{\max}, m_{\max}}^R - f_{n_{\max}, m_{\max}}^L > 0$
 - 11: Set $t_{m_{\max}}^{T,\max,(l)} = t_{m_{\max}}^{T,\max,(l-1)} - 1$ **if** $t_{m_{\max}+1}^{S,(l-1)} > t_{m_{\max}+1}^A + t_f^C$.
 - 12: Set $t_{n_{\max}}^{T,\max,(l)} = t_{n_{\max}}^{T,\max,(l-1)} + 1$ **if** $t_{n_{\max}}^{T,\max,(l-1)} < t_{n_{\max}}^A + C - t_{n_{\max}}^{S,(l-1)}$.
 - 13: **elseif** $f_{n_{\max}, m_{\max}}^R - f_{n_{\max}, m_{\max}}^L < 0$
 - 14: Set $t_{n_{\max}}^{T,\max,(l)} = t_{n_{\max}}^{T,\max,(l-1)} - 1$ **if** $t_{n_{\max}+1}^{S,(l-1)} > t_{n_{\max}+1}^A + t_f^C$.
 - 15: Set $t_{m_{\max}}^{T,\max,(l)} = t_{m_{\max}}^{T,\max,(l-1)} + 1$ **if** $t_{m_{\max}}^{T,\max,(l-1)} < t_{m_{\max}}^A + C - t_{m_{\max}}^{S,(l-1)}$.
 - 16: **else Break**
 - 17: **endif**
 - 18: Set $l = l + 1$.
 - 19: **end**
 - 20: Obtain the transmit power according to equation (28).
 - 21:
 - 22: **return** Transmit power of each subproblem.
-

Theorem 3. *If the optimal allowed transmission time of tasks $m, n \in \mathcal{I}_{t'}$ satisfies $t_i^S + t_i^{T,\max} \leq t_i^A + C, \forall i \in \{m, n\}$, then, it should also satisfy*

$$\frac{t_n^{T,\max}}{t_m^{T,\max}} = \frac{e^{\frac{D_m}{\tau W t_n^{T,\max}}} e^{\frac{1}{t_n^{T,\max}} \sum_{t=t_n^S}^{t_n^S + t_n^{T,\max}} \log(\tau W h_t^k)}}{e^{\frac{D_n}{\tau W t_m^{T,\max}}} e^{\frac{1}{t_m^{T,\max}} \sum_{t=t_m^S}^{t_m^S + t_m^{T,\max}} \log(\tau W h_t^k)}}, \forall n, m \in \mathcal{I}_{t'}. \quad (32)$$

Proof. Please refer to Appendix C. \square

Moreover, considering the constraints (30) and (31), we proposed an optimal algorithm to solve problem (P1-C) as shown in Algorithm 1.

3) *Restoration of transmit power:* With Algorithm 1, we can obtain the copies of transmit power at each time slot in all K subproblems, i.e., $\mathbf{p}_{t'}^k, \forall k \in \mathcal{K} \triangleq \{1, \dots, K\}$. In the following, we restore transmit power at each time slot from their copies, i.e., restoring $\mathbf{p}_{t'}$ from $\mathbf{p}_{t'}^k, \forall k \in \mathcal{K}$.

The ADMM can be leveraged for variable restoration, with a key finding being that it drives local copies of global variables towards their average value [30]–[32]. Particular, since the transmit power at each time slot is a continuous variable, it

Algorithm 2 Optimal algorithm for (P1-B)

- 1: **Initialization**
 - 2: • Input the number of samples K .
 - 3:
 - 4: Generate K subproblems based on K samples of channel coefficients.
 - 5: Obtain the solution of each subproblem by applying Algorithm 2.
 - 6: Restore transmit power at each time slot from their copies.
 - 7: **return** Solution of problem (P1-B).
-

can be restored by $\mathbf{p}_{t'} \approx \frac{1}{K} \sum_{k \in \mathcal{K}} \mathbf{p}_{t'}^k$. Therefore, the total algorithm for problem (P1-B) is shown in Algorithm 2.

V. SIMULATION RESULTS

In this section, we provide numerical examples to demonstrate the effectiveness of the proposed algorithm. We consider a UAV and a server, where the distance between them is set as $d = 100\text{m}$. The duration of each time slot is set as $\tau = 0.1\text{s}$. The receiver noise power and the channel power at the reference distance are set as $\sigma^2 = -110\text{dBm}$ and $\rho = -60\text{dB}$, respectively. Moreover, the bandwidth is set as $W = 2\text{MHz}$.

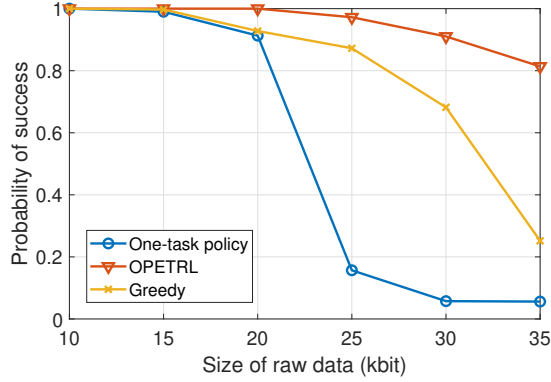
We compare the proposed OPETRL with the following two offloading policies.

- **One-task policy:** The policy optimizes the computation frequency and transmit power for each task independently, without taking into account the coupling among multiple sequential tasks.
- **Greedy:** The UAV chooses transmission mode and transmit power according to the current wireless channel parameters.

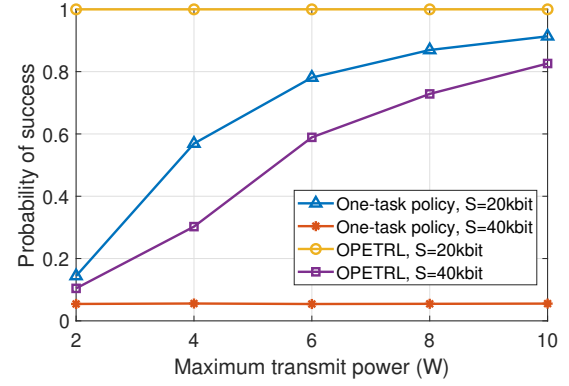
To reveal the effects of the size of raw data, we plot the probability of successful data transmission and the overall energy consumption versus the size of raw data in Fig. 3. From the numerical results, it can be obtained that the OPETRL generally outperforms the baselines. Moreover, both the proposed OPETRL and Greedy policy exhibit a slower decline in performance compared to that of the one-task policy.

For Fig. 3a, the increased size of the raw data results in an extended transmission time, thereby leading to a cascade of transmission failures for the later tasks when multiple tasks arrive intensively under the one-task policy. Thus, the probability of successful data transmission will fast decrease when the size of raw data is larger than 20 kbit. Moreover, the most of data transmission fails when $S \geq 25$ kbit under the one-task policy.

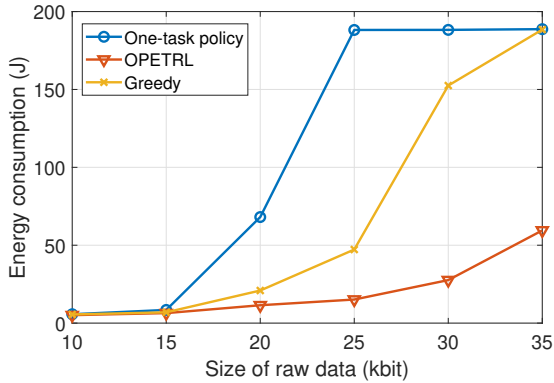
Similarly, as shown in Fig. 3b, the increased size of the raw data leads to a corresponding increase in overall energy consumption. This is because that the cascade of transmission failures results in the UAV transmitting data with maximum power most of the time. Meanwhile, the UAV will choose the CT pattern for most task, thereby consuming computational energy.



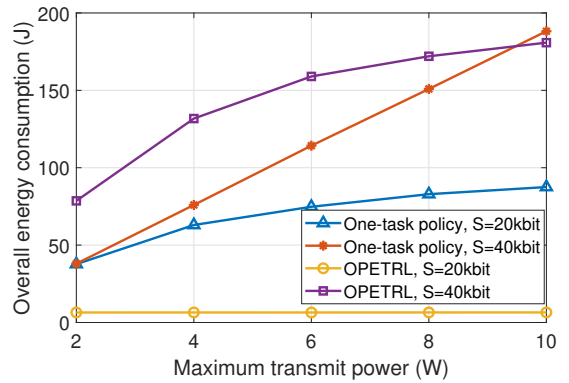
(a)



(a)



(b)



(b)

Figure 3. The effects of the size of raw data S . (a) The probability of successful data transmission versus S . (b) The overall energy consumption versus S .

Figure 4. The effects of the maximum transmit power P_{\max} . (a) The probability of successful task completion versus P_{\max} . (b) The overall energy consumption versus P_{\max} .

Furthermore, the impact of the maximum transmit power P_{\max} is depicted in Fig. 4. As we can see, when the size of raw data is small, the transmit power cannot significantly effect the probability of successful data transmission and the overall energy consumption under both the proposed OPETRL and the Greedy policy. This is attributed to the fact that the transmit power in both aforementioned policies is smaller than its maximum value. However, the UAV transmits data with maximum power most of the time when employing the one-task policy, a decrease in P_{\max} leads to a reduction in both the probability of successful data transmission and the overall energy consumption.

As shown in Fig. 4b, under one-task policy, a significant number of time slots remain idle while the maximum power is utilized for transmission. Hence, as the maximum power increases, there is a proportional increase in total energy consumption without any corresponding enhancement in the probability of successful task completion. However, OPETRL maximizes the utilization of time slots while ensuring that the transmit power in each slot remains below its maximum threshold. Therefore, an increase in the maximum transmit power results in a nearly logarithmical rise in total energy consumption.

VI. CONCLUSION

In this paper, a TRL-based architecture for multiple-task split inference in IoT networks is studied. The problem of minimizing overall energy consumption is initially formulated as a two-timescale optimization problem. Then, the problem is decomposed into two parts, where TRL is utilized to determine the transmission mode for each task and OP is used to optimize the transmit power in each time slot. Furthermore, we observe that the optimal transmit power decreases monotonically with increasing transmission time. Thus, the minimal transmit power is achieved by optimizing the transmission time of each task. Simulation results show that the proposed OPETRL can achieve a higher probability of successful data transmission with lower overall energy consumption.

APPENDIX

A. Proof of Theorem 1

By constructing the Lagrangian function of problem (P2), it can be obtained

$$\mathcal{L}(\mathbf{p}_{t_i^S}^k, \mu, \lambda, \xi, \eta) = \sum_{t=t_i^S}^{t_i^S+t_i^{\text{T,max}}} (p_t^k - \mu_t p_t^k + \lambda_t (p_t^k - p_{\max})) - \eta \left(\tau \left(\sum_{t=t_i^S}^{t_i^S+t_i^{\text{T,max}}} R_t^k \right) + D \right), \quad (33)$$

where μ_t and λ_t are the Lagrange multipliers associated with constraint (18), η is the Lagrange multipliers associated with constraint (27). Moreover, we define $\mu = (\mu_{t_i^S}, \dots, \mu_{t_i^S+t_i^{\text{T,max}}})$ and $\lambda = (\lambda_{t_i^S}, \dots, \lambda_{t_i^S+t_i^{\text{T,max}}})$. Therefore, the partial derivative of $\mathcal{L}(\mathbf{p}_{t_i^S}^k, \mu, \lambda, \xi, \eta)$ with respect to p_t^k is given by

$$\frac{\partial \mathcal{L}(\mathbf{p}_{t_i^S}^k, \mu, \lambda, \xi, \eta)}{\partial p_t^k} = 1 - \mu_t + \lambda_t - \eta \frac{\tau W h_t^k}{1 + h_t^k p_t^k}. \quad (34)$$

Then, the KKT conditions are written as follows

$$\frac{\partial \mathcal{L}(\mathbf{p}_{t_i^S}^{k,*}, \mu, \lambda, \xi, \eta)}{\partial p_t^{k,*}} = 0, \forall t \in \mathcal{T}_{t_i^S} \quad (35)$$

$$\mu_t p_t^{k,*} = 0, \lambda_t (p_t^{k,*} - p_{\max}) = 0, \forall t \in \mathcal{T}_{t_i^S} \quad (36)$$

$$\eta \left(\tau \left(\sum_{t=t_i^S}^{t_i^S+t_i^{\text{T,max}}} R_t^k(\mathbf{p}_{t_i^S}^{k,*}) \right) + D \right) = 0 \quad (37)$$

$$0 \leq p_t^{k,*} \leq p_{\max}, \forall t \in \mathcal{T}_{t_i^S} \quad (38)$$

$$\tau \sum_{t=t_i^S}^{t_i^S+t_i^{\text{T,max}}} R_t^k(\mathbf{p}_{t_i^S}^{k,*}) \geq D \quad (39)$$

$$\mu_t \geq 0, \lambda_t \geq 0, \forall t \in \mathcal{T}_{t_i^S}. \quad (40)$$

According to (34) and (35), we have

$$\eta = (1 - \mu_t + \lambda_t) \frac{1 + h_t^k p_t^{k,*}}{\tau W h_t^k}. \quad (41)$$

As a result, we consider the following three cases to analyze the optimal solution

- $\eta > \frac{1+h_t^k p_t^{k,*}}{\tau W h_t^k}$: It can be obtained that $1 - \mu_t + \lambda_t > 1$, i.e., $0 \leq \mu_t < \lambda_t$. Thus, we have $p_t^{k,*} = p_{\max}, \forall t \in \mathcal{T}_{t_i^S}$.
- $\eta < \frac{1+h_t^k p_t^{k,*}}{\tau W h_t^k}$: It can be obtained that $1 - \mu_t + \lambda_t < 1$, i.e., $0 \leq \lambda_t < \mu_t$. Thus, we have $p_t^{k,*} = 0, \forall t \in \mathcal{T}_{t_i^S}$.
- $\eta = \frac{1+h_t^k p_t^{k,*}}{\tau W h_t^k}$: It can be obtained that $1 - \mu_t + \lambda_t < 1$, i.e., $\lambda_t = \mu_t$. If $p_t^{k,*} = 0$, we have $0 \leq \mu_t < \lambda_t$, which is in conflict with $\lambda_t = \mu_t$; If $p_t^{k,*} = p_{\max}$, we have $0 \leq \lambda_t < \mu_t$, which is also contradictory. Hence, it can be obtained $0 < p_t^{k,*} < 1, \forall t \in \mathcal{T}_{t_i^S}$.

For the second case, if $p_t^{k,*} = 0, \forall t \in \mathcal{T}_{t_i^S}$, we have $\tau \sum_{t=t_i^S}^{t_i^S+t_i^{\text{T,max}}} R_t^k(\mathbf{p}_{t_i^S}^k) = 0$, which is in conflict with (39). Therefore, we have $\eta \geq \frac{1+h_t^k p_t^{k,*}}{\tau W h_t^k}$, i.e., For the third case, we have $\tau \sum_{t=t_i^S}^{t_i^S+t_i^{\text{T,max}}} R_t^k(\mathbf{p}_{t_i^S}^k) = D$ due to $\eta > 0$ and (37). Hence, it can be obtained

$$\tau \sum_{t=t_i^S}^{t_i^S+t_i^{\text{T,max}}} W \log(\eta \tau W h_t^k) = D. \quad (42)$$

Then, the Lagrange multipliers is given as

$$\eta = e^{\frac{\frac{D}{\tau W} - \sum_{t=t_i^S}^{t_i^S+t_i^{\text{T,max}}} (\tau W h_t^k)}{t_i^{\text{T,max}}}}. \quad (43)$$

Substituting (43) into $\eta = \frac{1+h_t^k p_t^{k,*}}{\tau W h_t^k}$, we can obtain

$$p_t^{k,*} = \tau W e^{\frac{\frac{D}{\tau W} - \sum_{t=t_i^S}^{t_i^S+t_i^{\text{T,max}}} \log(\tau W h_t^k)}{t_i^{\text{T,max}}}} - \frac{1}{h_t^k}. \quad (44)$$

The theorem is thus proved.

B. Proof of Theorem 2

Denote $\mathbf{p}_{t_i^S}^{k,*}$ as the optimal solution of problem (P2), while $\mathbf{p}_{t_i^S}^{k,'}$ is denoted as an another solution. Assume $p_{t_1}^{k,'} = p_t^{k,*}, \forall t \in (t_i^S, \dots, t_i^S+t_i^{\text{T,max}}) \setminus \{t_1, t_2\}$, where $0 < p_{t_1}^{k,*} < p_{\max}$ and $0 < p_{t_2}^{k,*} < p_{\max}$ with $t_1, t_2 \in (t_i^S, \dots, t_i^S+t_i^{\text{T,max}})$. Without loss of generality, let $p_{t_1}^{k,'} = 0$ and $p_{t_2}^{k,'} = p_{t_2}^{k,*} + \Delta p$ with $\Delta p > 0$. In other words, the transmission time of solution $\mathbf{p}_{t_i^S}^{k,'}$ is shorter than that of solution $\mathbf{p}_{t_i^S}^{k,*}$. As mentioned in Proof A, the optimal solution satisfies $\tau \sum_{t=t_i^S}^{t_i^S+t_i^{\text{T,max}}} R_t^k(\mathbf{p}_{t_i^S}^{k,*}) = D$. Therefore, we can obtain

$$\begin{aligned} & \log\left(1 + (p_{t_2}^{k,*} + \Delta p) h_{t_2}^k\right) - \log\left(1 + p_{t_2}^{k,*} h_{t_2}^k\right) \\ & \geq \log\left(1 + p_{t_1}^{k,*} h_{t_1}^k\right). \end{aligned} \quad (45)$$

Moreover, due to $0 < p_{t_2}^{k,*} < p_{\max}$, we have $\eta = \frac{1+h_{t_2}^k p_{t_2}^{k,*}}{\tau W h_{t_2}^k}$ according to the third case in Proof A. Hence, (45) can be written as

$$\begin{aligned} & \log(\eta \tau W h_{t_2}^k + \Delta p h_{t_2}^k) - \log(\eta \tau W h_{t_2}^k) \\ & \geq \log\left(1 + p_{t_1}^{k,*} h_{t_1}^k\right). \end{aligned} \quad (46)$$

We can obtain

$$\log\left(1 + \frac{\Delta p}{\eta \tau W}\right) \geq \log\left(1 + p_{t_1}^{k,*} h_{t_1}^k\right),$$

which can be rewritten as

$$\Delta p \geq p_{t_1}^{k,*} h_{t_1}^k \eta \tau W.$$

Similarly, $p_{t_1}^{k,*}$ and $h_{t_1}^k$ satisfy $\eta = \frac{1+h_{t_1}^k p_{t_1}^{k,*}}{\tau W h_{t_1}^k}$. Thus, we have $\Delta p \geq \left(1 + h_{t_1}^k p_{t_1}^{k,*}\right) p_{t_1}^{k,*} \geq p_{t_1}^{k,*}$, i.e., $\sum_{t=t_i^S}^{t_i^S+t_i^{\text{T,max}}} p_{t_1}^{k,*} \leq \sum_{t=t_i^S}^{t_i^S+t_i^{\text{T,max}}} p_{t_1}^{k,'}$. The theorem is thus proved.

C. Proof of Theorem 3

The objective function of problem (P3) can be written as

$$\begin{aligned} & \sum_{i \in \mathcal{I}_t'} E_i(t_i^{\text{T,max}}) \\ &= \sum_{i \in \mathcal{I}_t'} \sum_{t=t_i^{\text{S}}}^{t_i^{\text{S}}+t_i^{\text{T,max}}} \left(\tau W e^{\frac{\frac{D_i}{\tau W} - \sum_{t=t_i^{\text{S}}}^{t_i^{\text{S}}+t_i^{\text{T,max}}} \log(\tau W h_t^k)}{t_i^{\text{T,max}}}} - \frac{1}{h_t^k} \right). \end{aligned} \quad (47)$$

In (47), $\sum_{i \in \mathcal{I}_t'} \sum_{t=t_i^{\text{S}}}^{t_i^{\text{S}}+t_i^{\text{T,max}}} \frac{1}{h_t^k}$ is constant due to (30) and (31). Thus, our primary objective is to minimize the subtractor on the right-hand side in (47). Denote N_I as the number of tasks in set \mathcal{I}_t' . It can be obtained

$$\begin{aligned} & \sum_{i \in \mathcal{I}_t'} \sum_{t=t_i^{\text{S}}}^{t_i^{\text{S}}+t_i^{\text{T,max}}} \tau W e^{\frac{\frac{D_i}{\tau W} - \sum_{t=t_i^{\text{S}}}^{t_i^{\text{S}}+t_i^{\text{T,max}}} \log(\tau W h_t^k)}{t_i^{\text{T,max}}}} \\ & \geq N_I \sqrt{\prod_{i \in \mathcal{I}_t'} \left(\sum_{t=t_i^{\text{S}}}^{t_i^{\text{S}}+t_i^{\text{T,max}}} \tau W e^{\frac{\frac{D_i}{\tau W} - \sum_{t=t_i^{\text{S}}}^{t_i^{\text{S}}+t_i^{\text{T,max}}} \log(\tau W h_t^k)}{t_i^{\text{T,max}}}} \right)} \end{aligned} \quad (48)$$

The condition for equality of (48) is

$$\begin{aligned} & \sum_{t=t_n^{\text{S}}}^{t_n^{\text{S}}+t_n^{\text{T,max}}} e^{\frac{\frac{D_n}{\tau W} - \sum_{t=t_n^{\text{S}}}^{t_n^{\text{S}}+t_n^{\text{T,max}}} \log(\tau W h_t^k)}{t_n^{\text{T,max}}}} \\ &= \sum_{t=t_m^{\text{S}}}^{t_m^{\text{S}}+t_m^{\text{T,max}}} e^{\frac{\frac{D_m}{\tau W} - \sum_{t=t_m^{\text{S}}}^{t_m^{\text{S}}+t_m^{\text{T,max}}} \log(\tau W h_t^k)}{t_m^{\text{T,max}}}}, \forall n, m \in \mathcal{I}_t', \end{aligned} \quad (49)$$

which can be further written as

$$\begin{aligned} & t_n^{\text{T,max}} e^{\frac{\frac{D_n}{\tau W} - \sum_{t=t_n^{\text{S}}}^{t_n^{\text{S}}+t_n^{\text{T,max}}} \log(\tau W h_t^k)}{t_n^{\text{T,max}}}} \\ &= t_m^{\text{T,max}} e^{\frac{\frac{D_m}{\tau W} - \sum_{t=t_m^{\text{S}}}^{t_m^{\text{S}}+t_m^{\text{T,max}}} \log(\tau W h_t^k)}{t_m^{\text{T,max}}}}, \forall n, m \in \mathcal{I}_t'. \end{aligned} \quad (50)$$

Thus, we have

$$\begin{aligned} & \frac{t_n^{\text{T,max}}}{t_m^{\text{T,max}}} \\ &= \frac{e^{\frac{D_n}{\tau W t_m^{\text{T,max}}} - \frac{1}{t_m^{\text{T,max}}} \sum_{t=t_n^{\text{S}}}^{t_n^{\text{S}}+t_n^{\text{T,max}}} \log(\tau W h_t^k)}}{e^{\frac{D_m}{\tau W t_n^{\text{T,max}}} - \frac{1}{t_n^{\text{T,max}}} \sum_{t=t_m^{\text{S}}}^{t_m^{\text{S}}+t_m^{\text{T,max}}} \log(\tau W h_t^k)}}, \forall n, m \in \mathcal{I}_t'. \end{aligned} \quad (51)$$

REFERENCES

- [1] N. H. Motlagh, M. Baga, and T. Taleb, "Uav-based iot platform: A crowd surveillance use case," *IEEE Communications Magazine*, vol. 55, no. 2, pp. 128–134, 2017.
- [2] Y. Tan, J. Liu, and N. Kato, "Blockchain-based lightweight authentication for resilient UAV communications: Architecture, scheme, and future directions," *IEEE Wireless Communications*, vol. 29, no. 3, pp. 24–31, 2022.
- [3] D. Zhou, M. Sheng, B. Li, J. Li, and Z. Han, "Distributionally robust planning for data delivery in distributed satellite cluster network," *IEEE Transactions on Wireless Communications*, vol. 18, no. 7, pp. 3642–3657, 2019.
- [4] R. Liu, M. Sheng, K.-S. Lui, X. Wang, Y. Wang, and D. Zhou, "An analytical framework for resource-limited small satellite networks," *IEEE Communications Letters*, vol. 20, no. 2, pp. 388–391, 2016.
- [5] J. Shao and J. Zhang, "Communication-computation trade-off in resource-constrained edge inference," *IEEE Communications Magazine*, vol. 58, no. 12, pp. 20–26, 2020.
- [6] X. Liu, Y. Deng, and T. Mahmoodi, "Wireless distributed learning: A new hybrid split and federated learning approach," *IEEE Transactions on Wireless Communications*, vol. 22, no. 4, pp. 2650–2665, 2023.
- [7] T. Sun, X. Wang, M. Umehira, and Y. Ji, "Split learning assisted multi-UAV system for image classification task," in *2023 IEEE 97th Vehicular Technology Conference (VTC2023-Spring)*, 2023, pp. 1–6.
- [8] E. Li, L. Zeng, Z. Zhou, and X. Chen, "Edge AI: On-demand accelerating deep neural network inference via edge computing," *IEEE Transactions on Wireless Communications*, vol. 19, no. 1, pp. 447–457, 2020.
- [9] B. Atan, M. Basaran, N. Calik, S. T. Basaran, G. Akkuzu, and L. Durak-Ata, "AI-empowered fast task execution decision for delay-sensitive IoT applications in edge computing networks," *IEEE Access*, vol. 11, pp. 1324–1334, 2023.
- [10] S. Naveen, M. R. Kounte, and M. R. Ahmed, "Low latency deep learning inference model for distributed intelligent IoT edge clusters," *IEEE Access*, vol. 9, pp. 160 607–160 621, 2021.
- [11] X. Zhou, Y. Gao, C. Li, and Z. Huang, "A multiple gradient descent design for multi-task learning on edge computing: Multi-objective machine learning approach," *IEEE Transactions on Network Science and Engineering*, vol. 9, no. 1, pp. 121–133, 2022.
- [12] K. Guo, M. Sheng, J. Tang, T. Q. S. Quek, and Z. Qiu, "Exploiting hybrid clustering and computation provisioning for green c-ran," *IEEE Journal on Selected Areas in Communications*, vol. 34, no. 12, pp. 4063–4076, 2016.
- [13] X. Gu, G. Zhang, M. Wang, W. Duan, M. Wen, and P.-H. Ho, "Uav-aided energy-efficient edge computing networks: Security offloading optimization," *IEEE Internet of Things Journal*, vol. 9, no. 6, pp. 4245–4258, 2022.
- [14] K. Zeng, X. Li, and T. Shen, "Energy-stabilized computing offloading algorithm for uavs with energy harvesting," *IEEE Internet of Things Journal*, pp. 1–1, 2023.
- [15] F. Zhou, Y. Wu, R. Q. Hu, and Y. Qian, "Computation rate maximization in uav-enabled wireless-powered mobile-edge computing systems," *IEEE Journal on Selected Areas in Communications*, vol. 36, no. 9, pp. 1927–1941, 2018.
- [16] A. M. Seid, J. Lu, H. N. Abishu, and T. A. Ayall, "Blockchain-enabled task offloading with energy harvesting in multi-uav-assisted iot networks: A multi-agent drl approach," *IEEE Journal on Selected Areas in Communications*, vol. 40, no. 12, pp. 3517–3532, 2022.
- [17] D. Zhai, M. Sheng, X. Wang, Y. Li, J. Song, and J. Li, "Rate and energy maximization in scma networks with wireless information and power transfer," *IEEE Communications Letters*, vol. 20, no. 2, pp. 360–363, 2016.
- [18] Q. Lan, Q. Zeng, P. Popovski, D. GEndEz, and K. Huang, "Progressive feature transmission for split classification at the wireless edge," *IEEE Transactions on Wireless Communications*, vol. 22, no. 6, pp. 3837–3852, 2023.
- [19] X. Huang and S. Zhou, "Dynamic compression ratio selection for edge inference systems with hard deadlines," *IEEE Internet of Things Journal*, vol. 7, no. 9, pp. 8800–8810, 2020.
- [20] E. Li, L. Zeng, Z. Zhou, and X. Chen, "Edge AI: On-demand accelerating deep neural network inference via edge computing," *IEEE Transactions on Wireless Communications*, vol. 19, no. 1, pp. 447–457, 2020.
- [21] J. Yan, S. Bi, and Y.-J. A. Zhang, "Optimal model placement and online model splitting for device-edge co-inference," *IEEE Transactions on Wireless Communications*, vol. 21, no. 10, pp. 8354–8367, 2022.
- [22] Z. Hao, G. Xu, Y. Luo, H. Hu, J. An, and S. Mao, "Multi-agent collaborative inference via DNN decoupling: Intermediate feature compression and edge learning," *IEEE Transactions on Mobile Computing*, vol. 22, no. 10, pp. 6041–6055, 2023.
- [23] Y.-T. Yang and H.-Y. Wei, "Edge-IoT computing and networking resource allocation for decomposable deep learning inference," *IEEE Internet of Things Journal*, vol. 10, no. 6, pp. 5178–5193, 2023.
- [24] Y. Sun, D. Xu, D. W. K. Ng, L. Dai, and R. Schober, "Optimal 3D-trajectory design and resource allocation for solar-powered uav communication systems," *IEEE Transactions on Communications*, vol. 67, no. 6, pp. 4281–4298, 2019.
- [25] Y. Wang, M. Sheng, X. Wang, L. Wang, and J. Li, "Mobile-edge computing: Partial computation offloading using dynamic voltage scaling,"

- IEEE Transactions on Communications*, vol. 64, no. 10, pp. 4268–4282, 2016.
- [26] H. v. Hasselt, A. Guez, and D. Silver, “Deep reinforcement learning with double Q-learning,” in *Proceedings of the Thirtieth AAAI Conference on Artificial Intelligence*, ser. AAAI’16, 2016, pp. 2094–2100.
- [27] S. K. Kumar, “On weight initialization in deep neural networks,” *arXiv preprint arXiv:1704.08863*, 2017.
- [28] A. M.-C. So and Y. J. A. Zhang, “Distributionally robust slow adaptive OFDMA with soft qos via linear programming,” *IEEE J. Sel. Areas Commun.*, vol. 31, no. 5, pp. 947–958, 2013.
- [29] P. Yang, X. Xi, Y. Fu, T. Q. Quek, X. Cao, and D. Wu, “Multicast eMBB and bursty URLLC service multiplexing in a CoMP-enabled RAN,” *IEEE Trans. Wireless Commun.*, vol. 20, no. 5, pp. 3061–3077, 2021.
- [30] S. Boyd, N. Parikh, E. Chu, B. Peleato, J. Eckstein *et al.*, “Distributed optimization and statistical learning via the alternating direction method of multipliers,” *Foundations and Trends® in Machine Learning*, vol. 3, no. 1, pp. 1–122, 2011.
- [31] J. Tang, B. Shim, and T. Q. Quek, “Service multiplexing and revenue maximization in sliced C-RAN incorporated with URLLC and multicast eMBB,” *IEEE J. Sel. Areas Commun.*, vol. 37, no. 4, pp. 881–895, 2019.
- [32] H. Tabrizi, B. Peleato, G. Farhadi, J. M. Cioffi, and G. Aldabbagh, “Spatial reuse in dense wireless areas: A cross-layer optimization approach via ADMM,” *IEEE Trans. Wireless Commun.*, vol. 14, no. 12, pp. 7083–7095, 2015.